Article

Cell Reports

SAD-B Phosphorylation of CAST Controls Active Zone Vesicle Recycling for Synaptic Depression

Graphical Abstract

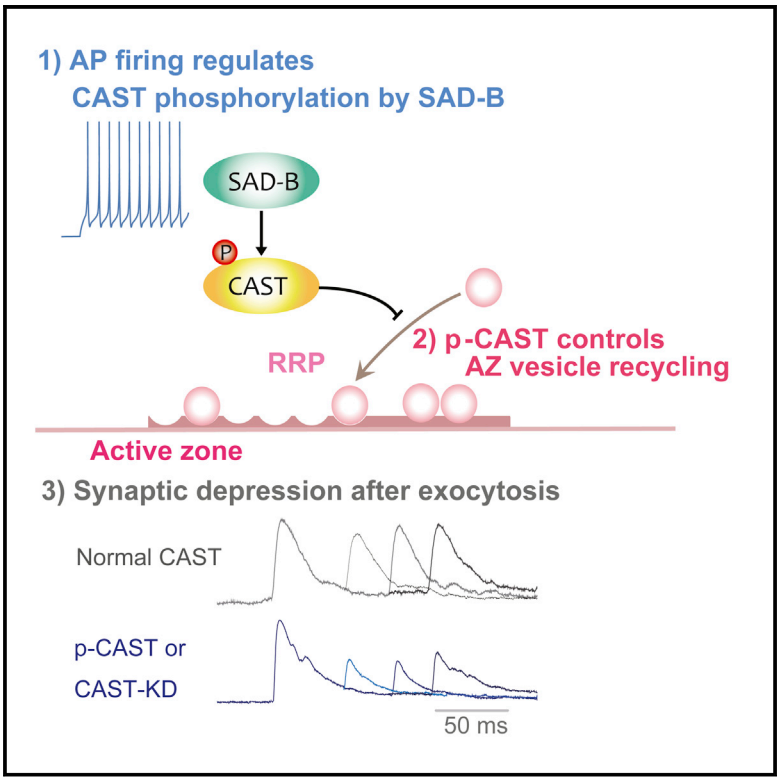

Highlights

- CAST S45 is phosphorylated by SAD-B or after presynaptic activity
- S45D CAST delays RRP reloading and enhances synaptic depression
- CAST deletion delays RRP reloading and enhances synaptic depression
- CAST phosphorylation provides temporal control of synaptic efficacy

Authors

Sumiko Mochida, Yamato Hida, Shota Tanifuji, ..., Isao Kitajima, Kenji Sakimura, Toshihisa Ohtsuka

Correspondence

mochida@tokyo-med.ac.jp (S.M.), tohtsuka@yamanashi.ac.jp (T.O.)

In Brief

Mochida et al. examine the molecular mechanisms underlying depression, an important form of synaptic plasticity. Their work shows that CAST, in concert with a protein kinase, SAD-B, regulates depression by controlling synaptic vesicle trafficking within presynaptic terminals. This pathway serves as a dynamic brake on synaptic transmission.

Mochida et al., 2016, Cell Reports *16*, 2901–2913
September 13, 2016
http://dx.doi.org/10.1016/j.celrep.2016.08.020

Cell Reports
Article

SAD-B Phosphorylation of CAST Controls Active Zone Vesicle Recycling for Synaptic Depression

Sumiko Mochida,[1,6,*] Yamato Hida,[2] Shota Tanifuji,[1] Akari Hagiwara,[2] Shun Hamada,[2] Manabu Abe,[3] Huan Ma,[1,5] Misato Yasumura,[2] Isao Kitajima,[4] Kenji Sakimura,[3] and Toshihisa Ohtsuka[2,*]
[1]Department of Physiology, Tokyo Medical University, Tokyo 160-8402, Japan
[2]Department of Biochemistry, Faculty of Medicine/Graduate School of Medicine, University of Yamanashi, Yamanashi 409-3898, Japan
[3]Department of Cellular Neurobiology, Brain Research Institute, Niigata University, Niigata 951-8585, Japan
[4]Department of Clinical and Molecular Pathology, Faculty of Medicine/Graduate School of Medicine, University of Toyama, Toyama 930-0194, Japan
[5]Present address: Department of Physiology, Institute of Neuroscience, Zhejiang University School of Medicine, Hangzhou 310058, China
[6]Lead Contact
*Correspondence: mochida@tokyo-med.ac.jp (S.M.), tohtsuka@yamanashi.ac.jp (T.O.)
http://dx.doi.org/10.1016/j.celrep.2016.08.020

SUMMARY

Short-term synaptic depression (STD) is a common form of activity-dependent plasticity observed widely in the nervous system. Few molecular pathways that control STD have been described, but the active zone (AZ) release apparatus provides a possible link between neuronal activity and plasticity. Here, we show that an AZ cytomatrix protein CAST and an AZ-associated protein kinase SAD-B coordinately regulate STD by controlling reloading of the AZ with release-ready synaptic vesicles. SAD-B phosphorylates the N-terminal serine (S45) of CAST, and S45 phosphorylation increases with higher firing rate. A phosphomimetic CAST (S45D) mimics CAST deletion, which enhances STD by delaying reloading of the readily releasable pool (RRP), resulting in a pool size decrease. A phospho-negative CAST (S45A) inhibits STD and accelerates RRP reloading. Our results suggest that the CAST/SAD-B reaction serves as a brake on synaptic transmission by temporal calibration of activity and synaptic depression via RRP size regulation.

INTRODUCTION

The active zone (AZ) beneath the presynaptic membrane is the principal site for Ca^{2+}-dependent exocytosis (Landis et al., 1988). The full molecular composition of the AZ is presently unclear, but many AZ proteins, including CAST/ERC2, ELKS, RIM1, Munc13-1, Piccolo/Aczonin, and Bassoon, have been identified (Brose et al., 1995; Fenster et al., 2000; Ohtsuka et al., 2002; Takao-Rikitsu et al., 2004; tom Dieck et al., 1998; Wang et al., 1997, 1999, 2002). Among AZ proteins, the highly homologous proteins CAST and ELKS play a key role in neurotransmitter release, representing the core of the AZ protein complex in mammalian synapses (Kaeser et al., 2009; Ohtsuka et al., 2002; Takao-Rikitsu et al., 2004; tom Dieck et al., 2012; Wang et al., 2002). However, how these proteins regulate neurotransmitter release remains unclear. Bruchpilot, a *Drosophila* ortholog of CAST and ELKS, is required for AZ structural integrity and Ca^{2+} channel clustering (Kittel et al., 2006; Wagh et al., 2006), suggesting a potential function for CAST/ELKS in the mammalian AZ. Indeed, CAST deletion in mice reduces AZ size in the retina (tom Dieck et al., 2012) and impairs inhibitory neurotransmission in the hippocampus (Kaeser et al., 2009). Bassoon, a binding partner of CAST and ELKS (Takao-Rikitsu et al., 2004), is involved in the reloading of synaptic vesicles (SVs) to release sites at excitatory synapses (Hallermann et al., 2010). Another binding partner, RIM1, interacts with Munc13-1 and has been implicated in SV docking (Wojcik and Brose, 2007) and priming (Betz et al., 2001). During synaptic plasticity, remodeling of the AZ related to Bruchpilot action has been suggested (Weyhersmüller et al., 2011). Therefore, several lines of evidence indicate that the CAST complex plays fundamental roles both in synaptic transmission and synaptic plasticity. However, the molecular mechanisms involved in functional regulation by CAST have not yet been elucidated.

Following firing of action potentials (APs), residual Ca^{2+} accumulates at the AZ and activates protein kinases (Zucker and Regehr, 2002) and Ca^{2+} binding proteins (Leal et al., 2012; Mochida, 2011; Mochida et al., 2008) that facilitate synaptic transmission. Among the numerous presynaptic kinases, protein kinase C reportedly regulates the reloading of SVs into the readily releasable pool (RRP) (Gillis et al., 1996) and also a short-term form of presynaptic plasticity, posttetanic potentiation (PTP) (Beierlein et al., 2007; Brager et al., 2003). For rapid remodeling of synaptic efficacy at the AZ, the phosphorylation of AZ protein(s) is ideal. Indeed, a previous study shows that an AZ-associated serine/threonine kinase, SAD, phosphorylates RIM1 (Inoue et al., 2006). RIM1 also is phosphorylated by PKA, another serine/threonine kinase (Lonart et al., 2003). However, recent genomic and proteomic analyses have revealed more than 600 protein kinases in humans (Manning et al., 2002). Therefore, we are only starting to understand the phosphorylation-signaling pathways that control the structure and function of the AZ.

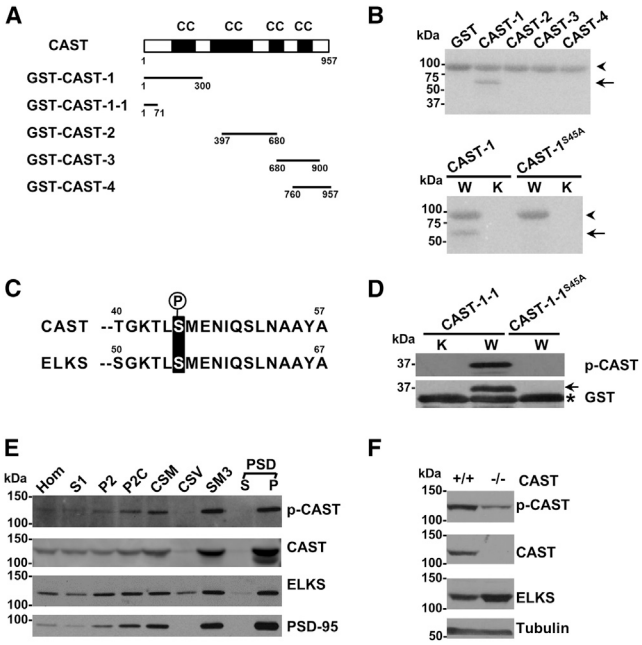

Figure 1. Biochemical Characterization of CAST Phosphorylation

(A) Various GST-tagged constructs of CAST. The numbers indicate aa residues. CC, coiled-coil domain.

(B) Identification of a phosphorylation site in CAST by SAD-B. Recombinant CAST fragment proteins were incubated with [γ-^{32}P] ATP and MBP-SAD-B kinase domain (KD) subjected to SDS-PAGE, followed by autoradiography (upper panel). S45 in CAST-1 was confirmed as the phosphorylation site by SAD-B (lower panel; W, WT of SAD-B KD; K, K63R mutant of it). Phosphorylation of CAST was not detected in runs with CAST-1^{S45A} in which serine 45 was replaced by alanine. Arrowheads indicate the position of autophosphorylated MBP-SAD-B KD. Arrows indicate the position of GST-CAST-1.

(C) Alignment of the phosphorylation sites in CAST and ELKS is shown.

(D) Production of an anti-phosphorylated CAST antibody (p-CAST). The antibody was raised against a peptide containing phosphorylated CAST^{S45}. Kinase assays were performed by incubation of MBP-SAD-B KD^{wild} or KD^{K63R} with recombinant GST-CAST that includes the phosphorylation site (CAST-1-1) in the presence of ATP. Each mixture was subjected to SDS-PAGE and western blotting with the anti-p-CAST (upper) and the anti-GST (lower) antibodies. The phosphorylation of CAST-1-1 by SAD-B caused the mobility shift of CAST-1-1 (arrow). Asterisk indicates the position of unphosphorylated GST-CAST-1-1 and -CAST1-1^{S45A}.

(E) Subcellular distribution. Rat brain homogenates were subjected to subcellular fractionation, and an aliquot of each fraction (10 μg) was analyzed by western blotting with the indicated antibodies. The results are representative of three independent experiments. Hom, homogenate; S1, crude synaptosomal fraction; P2, crude membrane fraction; P2C, synaptosomal fraction; CSM, crude synaptic membrane fraction; CSV, crude SV fraction; SM3, synaptosomal membrane; PSD, postsynaptic density fraction; S, 1% (w/v) Triton X-100-soluble fraction of PSD; P, 1% Triton X-100-insoluble fraction of PSD.

(F) In vivo phosphorylation of CAST and ELKS in the brain. Mouse brain homogenates of CAST WT and KO (10 μg of each) were analyzed by western blotting with the indicated antibodies. An immunoreactive band by the anti-p-CAST Ab was slightly observed in the CAST KO brain lysate, which suggests that ELKS also is phosphorylated in vivo.

Here we examined the phosphorylation of CAST in rat brain and sympathetic neurons, and we found that phosphorylated CAST is tightly associated with AZs. SAD-B, a synapse-associated kinase, phosphorylated CAST at its N-terminal serine residue (S45) in vitro. S45 phosphorylation increased when APs were elicited in sympathetic superior cervical ganglion (SCG) neurons. The expression of phosphomimetic CAST (S45D) reduced the number of SVs in the presynaptic RRP, delayed RRP reloading, and enhanced synaptic depression. In contrast, the expression of a phosphonegative CAST mutant (S45A) accelerated RRP reloading and reduced synaptic depression. CAST deletion mimicked the effects of phosphomimetic CAST. Our results indicate that rapid, activity-dependent inactivation of CAST by phosphorylation mediates short-term synaptic depression by regulating the rate of RRP reloading and, thereby, the number of SVs within the RRP.

RESULTS

Phosphorylation of CAST by SAD-B Kinase

Evidence suggests that CAST is a physiological determinant of the integrity of the AZ (Kaeser et al., 2009; Ohtsuka et al., 2002; Takao-Rikitsu et al., 2004; tom Dieck et al., 1998, 2012; Wang et al., 2002) and controls transmitter release (Takao-Rikitsu et al., 2004). Protein phosphorylation is regulated by synaptic activity (Browning et al., 1985; Nestler and Greengard, 1982); therefore, we investigated CAST phosphorylation as a potential mechanism for the modulation of synaptic transmission strength. Recent genomic proteomic analyses reveal more than 600 kinases in humans (Manning et al., 2002), suggesting that it may be impossible to identify specific kinase(s) for CAST phosphorylation. However, among synaptic kinases, one possible candidate is SAD-B, a kinase that is associated with SVs and the AZ and that phosphorylates the AZ protein RIM1 (Inoue et al., 2006).

To test whether SAD-B phosphorylates CAST, we first performed in vitro phosphorylation assays using various GST-tagged fragments of CAST (Figure 1A). GST-CAST-1 (amino acid [aa] 1–300) was specifically phosphorylated by SAD-B, whereas other investigated CAST regions were not (Figure 1B, top). Next, we identified the CAST phosphorylation site to be serine residue 45 (S45; Figure 1B, bottom), a residue that is conserved in the family member ELKS (Figure 1C). An anti-phosphorylated CAST (p-CAST) antibody confirmed that GST-CAST-1-1 (Figure 1A), but not GST-CAST-1-1^{S45A}, is phosphorylated by SAD-B (Figure 1D). This antibody also recognized phosphorylated ELKS at S55 (data not shown).

To examine CAST phosphorylation in vivo, we used the anti-p-CAST antibody to perform western blot analysis of subcellular fractionation samples. The protein band recognized by the antibody was concentrated and tightly associated with the postsynaptic density (PSD) fraction (Figure 1E), which contains both the AZ-cytomatrix and PSD components (Inoue et al., 2006): CAST, and the prominent PSD protein PSD-95, showed similar subcellular distribution, as previously reported (Ohtsuka et al., 2002). Moreover, we performed western blot analysis of brain lysates of CAST wild-type (WT) and knockout (KO) mice. The immunoreactive band was slightly detected in the CAST KO brain lysate (Figure 1F), possibly due to its cross-reactivity with phosphorylated ELKS and ELKS upregulation in the CAST KO mice (Figure 1F; see also tom Dieck et al., 2012). These results suggest that both CAST and ELKS

phosphorylation occur in vivo and that SAD-B kinase is responsible for these phosphorylations.

CAST^{S45} Phosphorylation Is Dependent on Membrane Excitability

Protein phosphorylation by neuronal activity is a general mechanism for regulating synaptic efficacy. To examine the relationship between the CAST^{S45} phosphorylation and presynaptic excitability, we used immunocytochemistry to visualize CAST^{S45} phosphorylation in cultured SCG neurons. SCG neurons in culture form an ideal model synapse for the functional study of presynaptic proteins (Mochida et al., 1994; Ma and Mochida, 2007). Using SCG neuron synapses, the presynaptic functions of CAST (Takao-Rikitsu et al., 2004) and SAD-B (Inoue et al., 2006) previously have been proposed in synaptic transmission. The antibody raised against phosphorylated CAST^{S45} recognized phosphorylated CAST^{S45}, but not CAST^{S45A} (Figures 2A and 2B; Figures S1–S3). Some synaptic boutons expressing CAST were stained with this antibody, likely indicating the presence of phosphorylated CAST^{S45} due to basal synaptic activity (Figure 2C). In comparison to the resting state, where phosphorylated CAST^{S45} was identified within synaptic boutons by Bassoon labeling (Figures 2C, and 2D), membrane excitation increased phosphorylation of CAST^{S45} (Figures 2E and 2F). Presynaptic AP trains at 20 or 50 Hz and membrane depolarization with high K^+ (40 mM) caused a 1.4-, 1.6- (Figure 2E), and 1.5-fold increase in phosphorylated CAST^{S45} (Figure 2F), respectively. This result suggests that neuronal activity induces CAST^{S45} phosphorylation.

Because the antibody against phosphorylated CAST^{S45} also cross-reacts with phosphorylated ELKS^{S55}, a close family member of CAST (Figures 1F and 2A), we cannot completely rule out the possibility that ELKS also might be phosphorylated upon neural activity. However, ELKS was rarely expressed at SCG synapses and rarely co-localized with Bassoon (Figures 2C and 2D), suggesting that ELKS is not a constituent of the core complex of AZ proteins in presynaptic terminals, at least in SCG neurons. Thus, it is likely that, at SCG synapses, CAST, but not ELKS, is phosphorylated with neuronal activity.

RRP Size Is Reduced by CAST Phosphorylation

We next investigated whether CAST^{S45} phosphorylation controls transmitter release. To examine the effects of CAST^{S45} phosphorylation on SV fusion, we expressed various EGFP-CAST forms in presynaptic SCG neurons. These included WT CAST (CAST^{WT}), as well as the phosphomimetic (CAST^{S45D}) and phosphonegative (CAST^{S45A}) mutants (Figure 3A). Punctate CAST and Bassoon signals co-localized at synaptic boutons surrounding the cell bodies of untransfected SCG neurons (Figure 2A; see also Takao-Rikitsu et al., 2004), whereas CAST^{WT} overexpression resulted in a donut-shaped distribution of Bassoon. These results indicate that CAST expression might regulate the distribution of Bassoon at presynaptic terminals. The five areas of Bassoon co-localizing with CAST^{WT}, 4.3 ± 0.19 μm^2, are 4.2 ± 1.1-fold greater than the area not co-localizing with CAST^{WT}, 1.3 ± 0.19 μm^2 (Figure 3A, bottom). CAST^{S45A} also increased the Bassoon areas to 4.4 ± 1.0-fold (five areas in an image), whereas fluorescence intensity of Bassoon was weaker in the areas where CAST^{S45D} was expressed. These results suggest that CAST overexpression should change AZ architecture and may modulate transmitter release.

To monitor the effects of these CAST proteins on transmitter release, excitatory postsynaptic potentials (EPSPs) were recorded from synaptically coupled neurons by stimulating transfected presynaptic neurons (Figures 3B–3E). Two days after transfection of CAST^{S45D}, the incidence of synaptic coupling, measured in four batches of cultures, decreased slightly (Figure 3B). The strength of synaptic transmission in CAST^{S45D}-transfected synapses, measured either as the peak amplitude or the integral of AP-evoked EPSPs, was about half of that measured in CAST^{WT}-transfected synapses (Figures 3C and 3D). The rise time of EPSP was slowed, and the half duration of EPSP was prolonged with CAST overexpression (Figure 3C). The mean integral value of averaged EPSP wave traces in CAST^{S45D} or CAST^{WT}-overexpressed synapses (Figure 3C) was 0.82, or 1.7-fold that in untransfected synapses, suggesting that CAST overexpression changed the size of the RRP of SVs or the number of release-ready SVs in the RRP. Release-ready SVs can be fused with the presynaptic membrane in response to an AP (i.e., release-ready SVs/RRP reflect the release probability [Del Castillo and Katz, 1954]).

The number of SVs in the RRP, estimated from the back-extrapolation (to time = 0) of cumulative EPSP area recorded at 50-Hz trains of 100 APs (Figures 3E and 3F), was 184 (CAST^{WT}), 123 (CAST^{S45A}), and 37 (CAST^{S45D}) compared to 84 ± 11 SVs previously estimated for the RRP of EGFP-expressing SCG neurons (Ma et al., 2009). Indeed, the mean integral value of the first EPSP was CAST^{WT} > CAST^{S45A} > CAST^{S45D} (Figure 3E), 30, 19, and nine vesicles within a 20-ms recording. Vesicle release probability (Del Castillo and Katz, 1954) was 0.27 (CAST^{WT}), 0.40 (CAST^{S45A}), and 0.75 (CAST^{S45D}), respectively, in contrast to 0.61 ± 0.08 previously measured in EGFP-expressing SCG neurons (Ma et al., 2009). Thus, the number of release-ready SVs in the RRP was 28 (CAST^{S45D}), 49 (CAST^{S45A}), and 50 (CAST^{WT}) in comparison to 49 (previously measured in EGFP-expressed neurons, Ma et al., 2009). These results indicate that CAST^{WT} or CAST^{S45A} overexpression did not change the number of primed vesicles, although the RRP size was increased by CAST^{WT} or CAST^{S45A} overexpression. In contrast, CAST^{S45D} decreased the size of the RRP and the number of release-ready SVs.

Interestingly, neither CAST^{WT} nor CAST^{S45D} changed the size of the SV pool (Figures 3H and 3I) or pool reloading (Figure 3J) when measured using 0.5 M sucrose (Figure 3G). A puff application every 4 min showed no rundown of EPSP in the SCG neurons (Mochida et al., 1998; Baba et al., 2005; Hayashida et al., 2015). The SV pool measured by 0.5 M sucrose was larger than the RRP measured by AP trains (Ma et al., 2009); the cumulative number of released SVs from synapses of untransfection, CAST^{WT}, CAST^{S45A}, or CAST^{S45D} overexpression at 2 s of the application was 418, 235, 332, and 571, respectively (Figure 3H). The values were 5.0-, 1.3-, 2.7-, and 15-fold, respectively, of the RRP size measured by AP trains, suggesting that unprimed vesicles in the RRP are decreased by CAST^{WT} or CAST^{S45A} overexpression and increased by CAST^{S45D} expression.

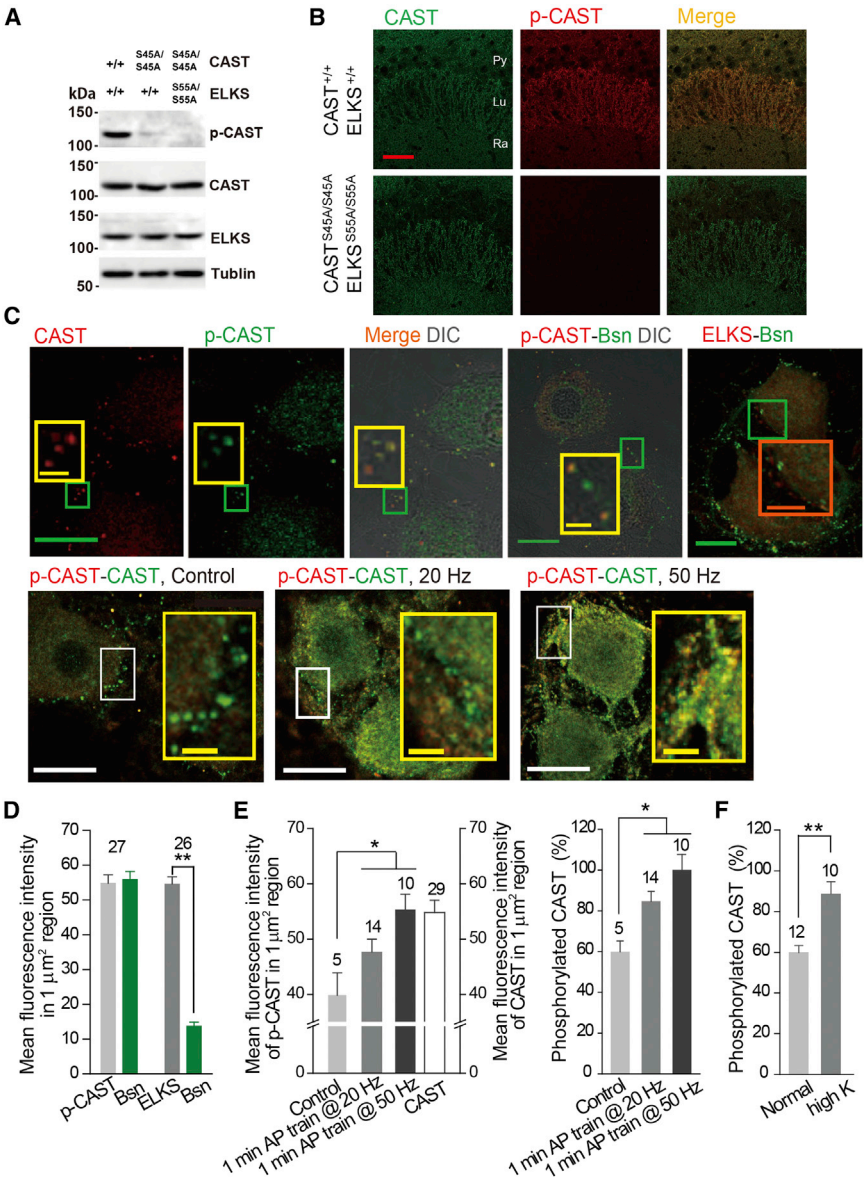

Figure 2. CAST Phosphorylation within SCG Neuron Synapses

(A) Specificity of the anti-p-CAST antibody was determined using CAST/ELKS double-knockin mice carrying the CAST S45A and ELKS S55A mutations. Brain lysates from WT, CAST^{S45A}, or the double mutant were subjected to subcellular fractionation to obtain the P2 fraction (2 μg for tubulin or 10 μg for other proteins), which was analyzed by western blotting with the indicated antibodies. An immunoreactive band detected by the anti-p-CAST antibody was completely abolished in the double-mutant sample, while a very faint immunoreactive band was observed in the CAST^{S45A} mouse sample.

(B) Immunohistochemistry using the anti-CAST and -p-CAST antibodies in the hippocampal CA3 region. In the control CAST$^{+/+}$/ELKS$^{+/+}$ mice, anti-CAST and -p-CAST antibody signals were observed and co-localized at St. Lucidum and Radiatum (upper panels). However, in the mutant CAST$^{S45A/S45A}$/ELKS$^{S55A/S55A}$ mice, the CAST signal was similar to controls and the p-CAST signal was completely abolished (lower panels). Scale bar, 50 μm.

(C) Co-localization of CAST and phosphorylated CAST (p-CAST) (upper left three panels) and localization of p-CAST and Bassoon and ELKS and Bassoon (upper right two panels) in normal Krebs' solution for 30 min. Co-localization shows CAST and p-CAST in non-stimulated control neurons (lower left), neurons stimulated with AP trains at 20 Hz for 1 min (lower middle), and at 50 Hz for 1 min (lower right). Insets are enlarged images of boxed areas. Yellow and orange dots in the merged images indicate synapses that co-localize p-CAST with CAST (merge differential interference contrast [DIC]) or with Bassoon (pCAST-Bsn DIC) or that co-localize ELKS with Bassoon (ELKS-Bsn). Green and white bars, 30 μm; yellow bar, 5 μm; orange bar, 15 μm.

(D–F) Mean fluorescence intensity within five regions (circle with 1 μm^2) around a cell body in a 180 × 180 μm^2 image containing two neurons was measured.

(D) Co-localization of phosphorylated CAST with Bassoon. Phosphorylated CAST was overlaid with Bassoon at a similar fluorescence intensity, whereas ELKS was rarely overlaid with Bassoon (**$p < 0.01$, unpaired Student's t test). Error bars represent SEM.

(E) Increase in phosphorylation of CAST with AP firing. (Left bar graph) Mean fluorescence intensity of p-CAST or CAST with and without an AP train is shown. Fluorescence intensity of CAST in the three different experimental conditions showed a similar value (right bar). (Right bar graph) Phosphorylated CAST (%) is shown. Values calculated from the ratio of fluorescence intensity of p-CAST to CAST in the three conditions are normalized by the value with the AP train at 50 Hz (mean ± SEM; *$p < 0.05$, Bonferroni post hoc test after one-way ANOVA versus control).

(F) Increase in the phosphorylation of CAST with high K$^+$. Phosphorylated CAST (%) was calculated from the ratio of fluorescence intensity of p-CAST to CAST in the normal and 40 mM K$^+$ Krebs' solution (high K$^+$) for 30 min (**$p < 0.01$, unpaired Student's t test). Error bars represent SEM.

RRP Reloading Is Delayed by Phosphorylated CAST

To examine whether CAST^{S45} phosphorylation regulates the speed of reloading of the RRP with SVs, we compared the rate of recovery from depletion of the RRP in synapses expressing CAST^{WT} or CAST^{S45} (Figure 4). The RRP was depleted by stimulating with a train of 1,500 APs at a low rate (5 Hz) to avoid inducing forms of activity-dependent synaptic plasticity, such as augmentation and PTP (Mochida et al., 2008), while monitoring RRP recovery by measuring the amplitude of EPSP recorded at 0.5 Hz (Figures 4A–4D). Our previous work showed that RRP recovery in SCG neurons consists of two phases: a fast component that corresponds to rapid reloading of the RRP with SVs from the reserve pool (RP) and a slow component that is based on the gradual reloading of the RRP with SVs generated through endocytic pathways (Lu et al., 2009; Tanifuji et al., 2013). It is noteworthy that the RRP recovery was not completed

10 min after the SV pool depletion with 1,500 APs (5 Hz) (Figure 4D), suggesting that the recycling pool (Rizzoli and Betz, 2005) is not able to fully recover after intense firing activity with 0.5 Hz EPSP monitoring that reduces the release-available SVs (Mochida et al., 1994).

The fast recovery rate is estimated by an exponential fit to the increase in EPSP amplitude (n = 4–7) measured from 0 to 8 s after the depleting stimulus train (Figure 4E), while the slow recovery rate is calculated by a linear fit to the recovery of EPSP amplitudes between 40 and 300 s (Figure 4F). The time constant (τ) for the fast recovery rate was 1.5 ± 0.8 s for CAST^{WT}, 3.2 ± 1.1 s for CAST^{S45A}, and 2.2 ± 0.9 s for untransfected synapses. Thus, CAST^{WT} accelerated the fast recovery rate (Figure 4E), while CAST^{S45A} slowed it ($p < 0.001$, Bonferroni post hoc test after one-way ANOVA, CAST^{WT} or CAST^{S45A} versus untransfected synapses). However, the degree of recovery during the fast component was 2.1-fold greater for CAST^{S45A} than for untransfected neurons (Figure 4E). Indeed, the recovery time of CAST^{S45A} to the plateau level of untransfected synapses (2.2 s) was much faster than that of untransfected synapses (8 s), suggesting that CAST^{S45A} accelerated the RRP reloading rate. In contrast, the recovery rate immediately after SV depletion was much slower for CAST^{S45D} than for CAST^{S45A} (Figure 4E). The slow recovery rate was 1.5%/min for CAST^{WT}, 3.7%/min for CAST^{S45A}, and 2.7%/min for untransfected synapses (Figure 4F) ($p < 0.001$, Bonferroni post hoc test after one-way ANOVA). The fact that CAST^{S45A} accelerated the slow recovery component suggests that CAST phosphorylation slows recovery. Consistent with this, CAST^{S45D} delayed the slow recovery phase to 0.023%/min ($p < 0.001$, Bonferroni post hoc test after one-way ANOVA). These results suggest that CAST^{S45} phosphorylation decreases RRP size by slowing SV reloading during and after intense synaptic activity.

Phosphorylation of CAST Controls Rapid RRP Reloading

To examine the time window for phosphorylated CAST to control SV reloading, we used a paired-pulse stimulation protocol (Figure 5A). As in untransfected synapses (Lu et al., 2009; Mori et al., 2014), in CAST^{WT}-overexpressing synapses, the second EPSP generated 30–120 ms after the first AP was smaller than the first EPSP. This is because of synaptic depression. CAST^{S45A} decreased synaptic depression, suggesting that phosphorylated CAST^{S45} downregulates RRP reloading shortly (inter-stimulus interval [ISI] < 200 ms) after an AP but not over longer (ISI > 200 ms) time courses. In contrast, CAST^{S45D} decreased the amplitude of the second EPSP at ISIs ranging from 50 to 2,000 ms (Lu et al., 2009; Mori et al., 2014), confirming that reloading of the RRP is downregulated by CAST phosphorylation. The decreased amplitude of the second EPSP evoked at ISIs > 200 ms (Figure 5A) suggests that CAST^{S45D} can control RRP reloading; however, in untransfected synapses, dephosphorylated CAST cannot control RRP reloading when ISIs > 200 ms are used. Thus, phosphorylated CAST negatively controls RRP reloading within 200 ms of AP firing.

Changes in paired-pulse amplitude ratios (PPRs) could reflect either a change in basal release probability prior to stimulation or an activity-dependent change in release probability in response to stimulation. When PPRs are altered by changes in basal release probability, then the PPR is inversely proportional to the amplitude of the first EPSP, which depends on the basal release probability (Zucker and Regehr, 2002). Thus, the enhanced depression during paired-pulse stimulation observed at synapses expressing CAST^{S45D} may be related to an increased release probability (0.75 versus 0.61 in untransfected neurons [Ma et al., 2009]) along with a decreased RRP size (37 vesicles versus 84 vesicles in untransfected neurons [Ma et al., 2009]). In contrast, CAST^{S45A} reduced depression at short ISIs (<200 ms; Figure 5), suggesting that phosphorylated CAST increases release probability shortly after AP generation by decreasing RRP size. Thus, phosphorylation of CAST changes synaptic depression.

CAST Deletion Mimics CAST Phosphorylation

Although CAST deletion in mice reduced the AZ size in the retina (tom Dieck et al., 2012), no ultrastructural changes were observed in central synapses (Kaeser et al., 2009). To examine the physiological significance of CAST phosphorylation, we knocked down CAST in presynaptic SCG neurons using two different small hairpin RNAs (shRNAs) (5′-GCTTGAAACCCT TAGCAAT-3′, shRNA1392; and 5′-GCAACACATTGAAGTGC TT-3′, shRNA1428), and we applied the same protocols to measure RRP reloading (Figures 4I–4K and 5B). These shRNAs, but not control shRNA (5′-GAAACGGAAAGCAGGTACG-3′), strongly reduced CAST expression in HEK293T cells (Figures 4G and 4H). Deletion of CAST showed no significant reduction in EPSP amplitude (CAST-control-shRNA, 32.3 ± 5.5 mV [n = 10]; CAST-1392-shRNA, 32.3 ± 4.8 mV [n = 12]; and CAST-1428-shRNA, 30.5 ± 4.1 mV [n = 11]), consistent with a previous study of ELKS2α deletion in excitatory synapses (Kaeser et al., 2009). However, the rate of the fast reloading phase following RRP depletion was delayed by CAST deletion (Figures 4I–4O). Indeed, paired-pulse depression was facilitated by CAST deletion (Figure 5B). These results suggest that the inactivation of CAST by phosphorylation mediates synaptic depression in excitatory synapses during high-frequency AP firing.

Short-Term Plasticity Is Suppressed by Phosphorylated CAST

We examined the possible contribution of phosphorylated CAST to two other forms of short-term presynaptic plasticity, augmentation and PTP (Zucker and Regehr, 2002), by monitoring synaptic transmission after a train of APs. Augmentation was evoked by 10-s-long AP trains and PTP with 60-s AP trains at frequencies of 20 and 40 Hz (Figure 6A). To prevent postsynaptic AP generation and reduce synaptic depression, external Ca^{2+} concentration was reduced from the normal 2.5 to 1 mM. Augmentation was observed after 10-s AP trains (70% ± 17% and 120% ± 65% increase; $p < 0.01$, paired Student's t test; n = 7; Figure 6B) at synapses overexpressing CAST^{WT}, similar to that observed in untransfected neurons. While CAST^{S45A} had no effect on the magnitude of augmentation (Figure 6B), CAST^{S45D} significantly reduced augmentation ($p < 0.05$, versus WT or untransfected, unpaired Student's t test). These data demonstrate that CAST phosphorylation is not required for the generation of augmentation, although augmentation is inhibited when CAST^{S45} is phosphorylated.

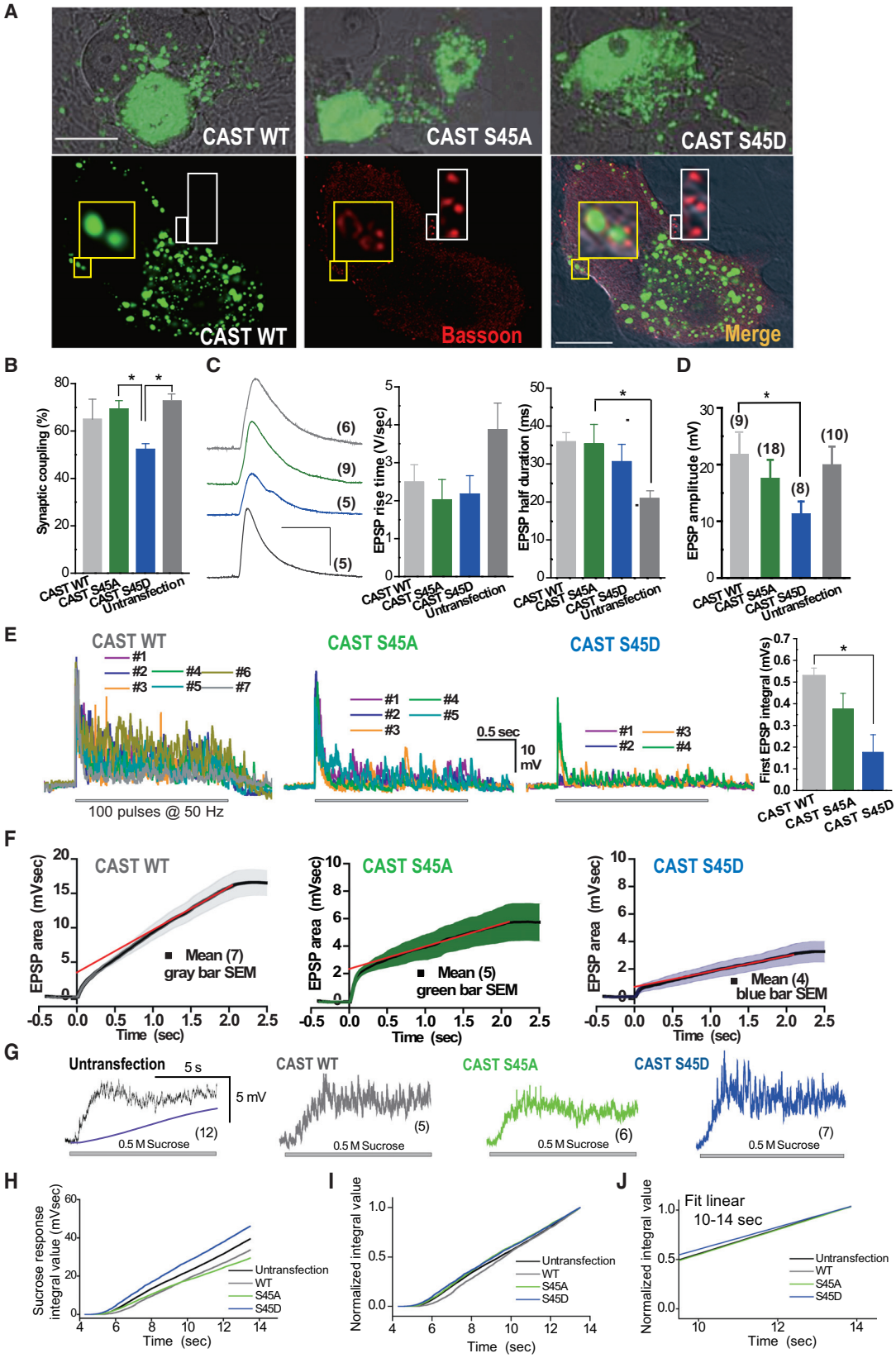

(legend on next page)

CAST^{S45D} showed a small but non-significant reduction in the magnitude of PTP elicited by 60-s AP trains (Figure 6B), suggesting that phosphorylated CAST^{S45} is not involved in this slower form of synaptic enhancement. We conclude that the phosphorylation of CAST is not involved in augmentation and PTP, suggesting that the Ca^{2+} signal for the generation of augmentation or PTP does not activate the CAST phosphorylation pathway. However, the Ca^{2+} concentration is critical for CAST function in generating augmentation or PTP (Figure 6C), although CAST has no Ca^{2+}-binding site.

Ca^{2+} Dependence of CAST Function

To examine the role of Ca^{2+} in CAST function, we varied extracellular Ca^{2+} concentration while measuring SV release efficacy in response to trains of ten APs at 5, 10, and 20 Hz (Figure 7A). Each AP train was applied three times, at 1-min intervals, for each extracellular Ca^{2+} concentration. CAST^{WT}, CAST^{S45A}, or CAST^{S45D} decreased transmitter release (Figure 7A) and increased EPSP failure during repetitive stimulation at low Ca^{2+} concentrations (Figure 7B). These data indicate that CAST impairs SV release efficacy in low Ca^{2+} conditions. Consistent with this interpretation, synaptic facilitation was prevented with CAST^{WT}, CAST^{S45A}, or CAST^{S45D} expression. In untransfected neurons, consistent with previous observations (Baba et al., 2005), EPSPs generated by the second presynaptic AP (ISI = 50 ms) were facilitated at low Ca^{2+} (0.5 or 0.2 mM), while CAST^{WT} or CAST^{S45} mutants showed no such facilitation (Figure 7A). Together, our results suggest that some other Ca^{2+}-dependent regulation of CAST, beyond the phosphorylation of CAST^{S45}, is involved in the regulation of SV release efficacy to maintain synaptic transmission during high rates of activity.

DISCUSSION

In the present study, we demonstrated that the temporal regulation of SV release efficacy at the AZ is controlled by the phosphorylation of CAST^{S45}. Phosphorylated CAST^{S45} downregulated SV reloading into the RRP within 200 ms following AP input (Figure 5). Phosphorylated CAST^{S45} also slowed the rate of RRP reloading (Figure 4) and decreased RRP size (Figure 3), resulting in greater synaptic depression during high rates of synaptic activity (Figure 5). CAST^{S45} was phosphorylated by SAD-B (Figure 1), and the phosphorylation of CAST^{S45} in SCG neuron synaptic boutons was strongly increased by presynaptic firing rate (Figure 2). Thus, we propose that rapid, activity-dependent CAST^{S45} phosphorylation mediates short-term synaptic depression by controlling SV reloading into the RRP and the number of SVs in the RRP. When CAST^{S45} phosphorylation was prevented, CAST upregulated the number of SVs reloaded into the RRP within 200 ms following an AP (Figure 5). CAST^{S45A} accelerated RRP reloading rate (Figure 4), thereby reducing synaptic depression during high rates of activity (Figure 5). CAST deletion mimics CAST^{S45} phosphorylation (Figures 4 and 5), suggesting that the inactivation of CAST by phosphorylation mediates short-term synaptic depression.

CAST Phosphorylation by SAD-B Kinase

We show that SAD-B, known to be associated with SVs and the AZ cytomatrix, directly phosphorylates CAST. Although we cannot rule out possible additional postsynaptic actions, our biochemical (Figure 1) and immunocytochemical data (Figure 2), taken together with previous work (Inoue et al., 2006), suggest that SAD-B phosphorylates CAST in presynaptic terminals. Mechanistically, SAD-B can potently phosphorylate CAST N-terminal S45. Our experiments with recombinant kinase domains suggest that the region containing CAST S45 is a previously uncharacterized consensus motif for phosphorylation by SAD kinases.

At present, the upstream signaling pathways for SAD-B-mediated phosphorylation are unknown. Because membrane depolarization increased CAST phosphorylation in vivo (Figure 2), one such candidate signal is Ca^{2+}, which is known to be essential for short-term presynaptic plasticity (Leal et al., 2012; Mochida, 2011; Mochida et al., 2008). So far, liver kinase B (LKB1) and

Figure 3. CAST^{S45} Overexpression Modulates RRP Size

(A) DIC and EGFP images of SCG neurons 2 days after transfection with CAST and CAST^{S45} mutant (upper three panels). EGFP image of CAST^{WT}, immunofluorescent images of Bassoon, and merged DIC image (lower panels) are shown. Insets are enlarged images of boxed areas (×10). Yellow box shows co-localization of CAST^{WT} and Bassoon while white box shows Bassoon.

(B) Incidence of synaptic coupling from the CAST- or CAST^{S45} mutant-transfected neuron to a neighboring untransfected neuron in four batches of cultures (mean ± SEM; *$p < 0.05$, unpaired t test; $p > 0.05$, Bonferroni post hoc test after one-way ANOVA). Total trials for CAST^{WT}-, CAST^{S45A}-, CAST^{S45D}-, and non-transfected neuron pairs were 35, 41, 62, and 43, respectively.

(C) Averaged EPSP traces in response to ten APs in the CAST-transfected presynaptic neuron were averaged. The values from neuron pairs indicated in parentheses were averaged. The rise time and half duration were calculated from the averaged EPSP trace of each neuron pair (*$p < 0.05$, Bonferroni post hoc test after one-way ANOVA). Vertical bar, 10 mV; horizontal bar, 50 ms. Error bars represent SEM.

(D) Averaged EPSP amplitudes are shown (*$p < 0.05$, Bonferroni post hoc test after one-way ANOVA). Error bars represent SEM.

(E) EPSP in response to 50-Hz train of 100 APs is shown. Error bars represent SEM.

(F) Averaged cumulative EPSP integral values with SEM (gray bars, WT; green bars, S45A; and blue bars, S45D) were calculated from the EPSP traces shown in (E). The red line represents a linear regression fit to data points from 1 to 2 s to estimate the integral value at time 0, indicating the RRP size. The number of SVs in the RRP, estimated by dividing the value at t = 0 by the mean cumulative integral value of the quantal EPSP (0.019 mV), was 184, 127, or 37 vesicles in CAST^{WT}-, CAST^{S45A}-, and CAST^{S45D}-transfected neurons. The number of experiments is indicated in parentheses.

(G) Averaged postsynaptic sucrose responses. Sucrose (0.5 M) was puff-applied for 10 s with nitrogen pressure to presynaptic terminals of untransfected, CAST-, or CAST^{S45} mutant-transfected neurons. Five averaged recordings with 4-min intervals in each synapse were averaged (n = 5–12). The baseline shown within the left trace is an averaged recording that did not show an EPSP with puff application of sucrose (n = 5).

(H) Cumulative integral value of averaged postsynaptic sucrose responses in (G) is shown.

(I) Normalized cumulative integral value of averaged postsynaptic sucrose responses in (G) is shown.

(J) The linear fit slopes from the values at 10 to 14 s for the normalized cumulative integral value in (I) are shown.

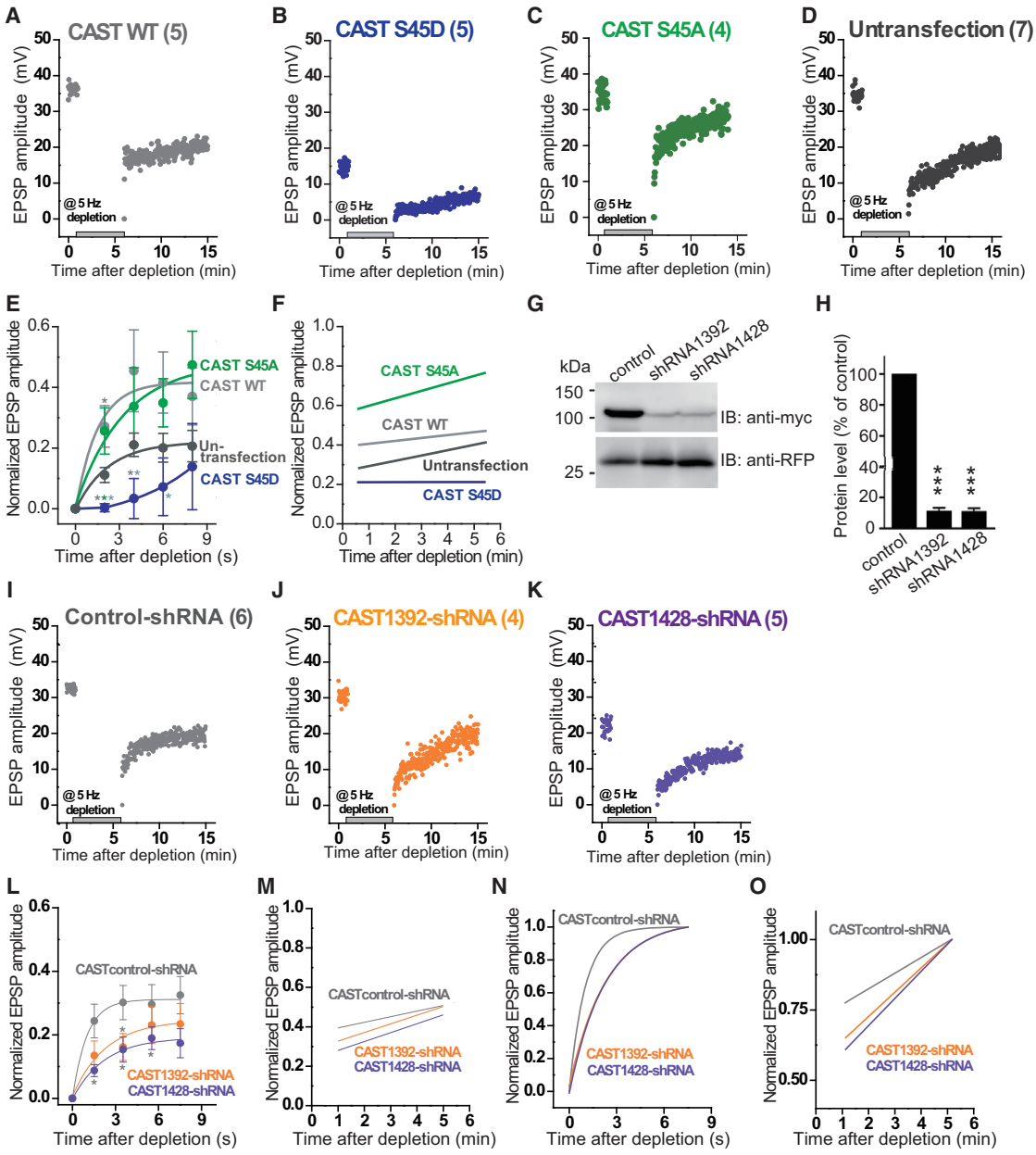

Figure 4. CAST^{S45A} Accelerated RRP Recovery, whereas CAST^{S45D} or CAST Depletion Delayed Recovery

(A–D and I–K) EPSPs were recorded at 0.5 Hz. A 5-min train of APs at 5 Hz was applied, as indicated, to deplete releasable SVs from the RRP. EPSP amplitudes were normalized to the averaged EPSP amplitude measured for 1 min before application of the train. EPSP amplitude recovered with two different rates, fast and slow phases, after the cessation of SV depletion is shown. The number of experiments is indicated in parentheses.

(E and L) The fast recovery rate is estimated by an exponential fit to the increase in EPSP amplitude from 0 to 8 s after depletion. The averaged EPSP amplitudes are the same as those shown in (A–D) (E) and (I–K) (L). Error bars represent SEM (*$p < 0.05$; EPSP amplitudes, unpaired Student's t test (E and L), and recovery curves, Bonferroni post hoc test after one-way ANOVA (L).

(F and M) The slow recovery rate can be estimated by a linear fit to recovering EPSP amplitudes from 60 to 300 s after the depletion shown in (A)–(D) (F) and (I)–(K) (M).

(G and H) The shRNA-mediated knockdown of CAST in HEK293T cells. Three days after co-transfection with pCIneo-myc-rCAST, proteins were extracted and subjected to immunoblot analysis (G). The intensities of bands for CAST were quantified and normalized with those for RFP (H).

(N) Single exponential curves shown in (L) are normalized to the value at 8 s.

(O) Linear fit slopes shown in (M) are normalized to the value at 5 min.

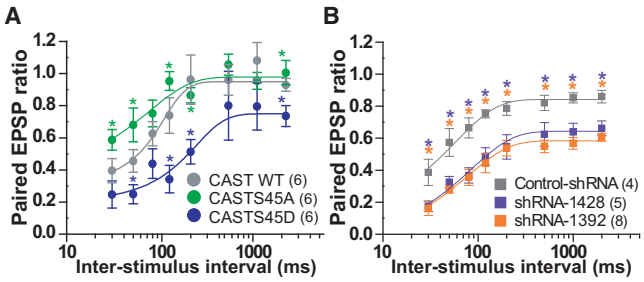

Figure 5. CAST^{S45A} Reduced Paired-Pulse Depression, whereas CAST^{S45D} or CAST Deletion Increased Depression

(A and B) Paired EPSP ratio plotted against ISI. Paired EPSP ratio equals the amplitude of the second EPSP divided by the amplitude of the first EPSP (*p < 0.05, unpaired t test, A, or Bonferroni post hoc test after one-way ANOVA, B; green *, CAST^{S45A} versus CAST^{S45D}; blue *, CAST^{S45D} versus CAST^{WT} transfection; violet *, control-shRNA versus CAST1428-shRNA; orange *, control-shRNA versus CAST1392-shRNA transfection). The number of experiments is indicated in parentheses. Error bars represent SEM.

calmodulin-dependent protein kinase kinase β (CaMKKβ) are the major known upstream regulators for SAD kinases (Hardie, 2007). Thus, CaMKKβ may be upstream of SAD-B, leading to the phosphorylation of CAST and the regulation of synaptic efficacy. In contrast to the short-term regulation of synaptic efficacy by CAST phosphorylation in SCG neurons, hippocampal CA1 synapses in CaMKKβ-null mutant mice have impaired long-term potentiation and normal paired-pulse facilitation and input-output ratio (Peters et al., 2003).

CAST Controls Basal Transmitter Release

Our results demonstrate that CAST overexpression increases RRP size; the estimated number of SVs in the RRP is 184 for CAST^{WT} and 123 for CAST^{S45A}, both of which are larger than the previous estimate of 84 SVs in the RRP of SCG neurons (Ma et al., 2009). However, CAST did not change the number of release-ready SVs in the RRP (≈50) or SV release efficacy (Figure 3). The level of neurotransmitter release is the product of two parameters (Del Castillo and Katz, 1954): the number of release-ready SVs (N) and vesicular release probability (p_{vr}). Synaptic release probability (p_{syn}, the probability that at least one vesicle is released per synapse) is related to these two parameters according to $p_{syn} = 1 - (1 - p_{vr})^N$ (Hanse and Gustafsson, 2001). Synaptic release probability corresponds to the number of docked vesicles and the number of release-ready SVs in the RRP (Branco et al., 2010; Schikorski and Stevens, 2001). Our present data suggest that CAST expression controls the level of neurotransmitter release by regulating the RRP size, without changing the number of release-ready SVs in the RRP but rather by changing the temporal synchronization of SV discharge (Figure 3C). Thus, CAST regulates the temporal efficacy of synaptic transmission.

The deletion of AZ proteins can alter neurotransmitter release, indicating a significant role for such proteins in basal transmitter release. RRP size and vesicular release probability in hippocampal excitatory synapses are upregulated by RIM1α (Calakos et al., 2004; Schoch et al., 2002), a docking (Han et al., 2011) and priming factor (Deng et al., 2011) for SVs, and Munc13-2, another priming factor (Rosenmund et al., 2002). In contrast,

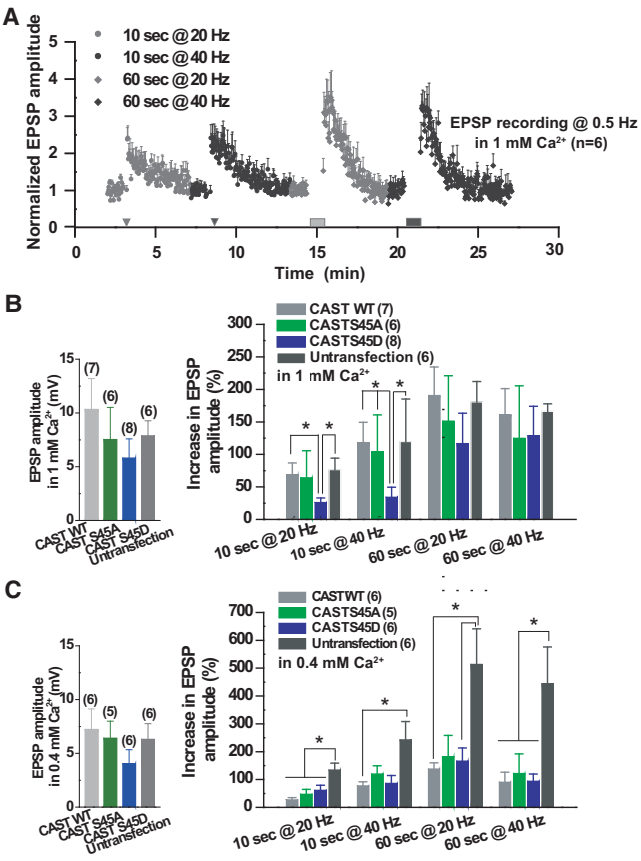

Figure 6. CAST^{S45D} Reduced Synaptic Augmentation

(A) Augmentation and posttetanic potentiation (PTP) of EPSP recorded from untransfected synapses. EPSP was recorded every 2 s in 1 mM Ca^{2+}. Conditioning stimuli of 20 and 40 Hz AP trains were applied at the indicated times to generate augmentation (for 10 s) and PTP (for 60 s). EPSP amplitudes were normalized to the averaged EPSP amplitude measured for 1 min before the conditioning stimuli. The values from six experiments were averaged.

(B and C) Augmentation and PTP of EPSP recorded from transfected synapses in 1 mM (B) or 0.4 mM Ca^{2+} (C). EPSP amplitudes for 1 min after a conditioning stimulus were averaged and normalized to the averaged EPSP amplitude measured for 1 min before the conditioning stimulus shown in the left bar graphs. The normalized values of each experiment were averaged and expressed as percentage increase (*p < 0.05, unpaired t test). The number of experiments for CAST^{WT} or CAST^{S45} mutant transfection is indicated in parentheses. Error bars represent SEM.

RRP size and vesicular release probability are downregulated by CAST in inhibitory, but not in excitatory, synapses of CA1 pyramidal neurons (Kaeser et al., 2009). Our study demonstrates that CAST^{S45} phosphorylation, but not ELKS phosphorylation, also downregulates RRP size and the number of release-ready SVs within 200 ms following AP firing in excitatory cholinergic synapses in sympathetic neurons (Figures 3E and 3F), suggesting a specificity in AZ protein subcomplex regulation.

CAST Rapidly Modulates Short-Term Synaptic Plasticity

The genetic deletion of AZ proteins has suggested their significant roles in presynaptic short-term plasticity, such as paired-pulse facilitation (RIM1α [Calakos et al., 2004; Schoch et al.,

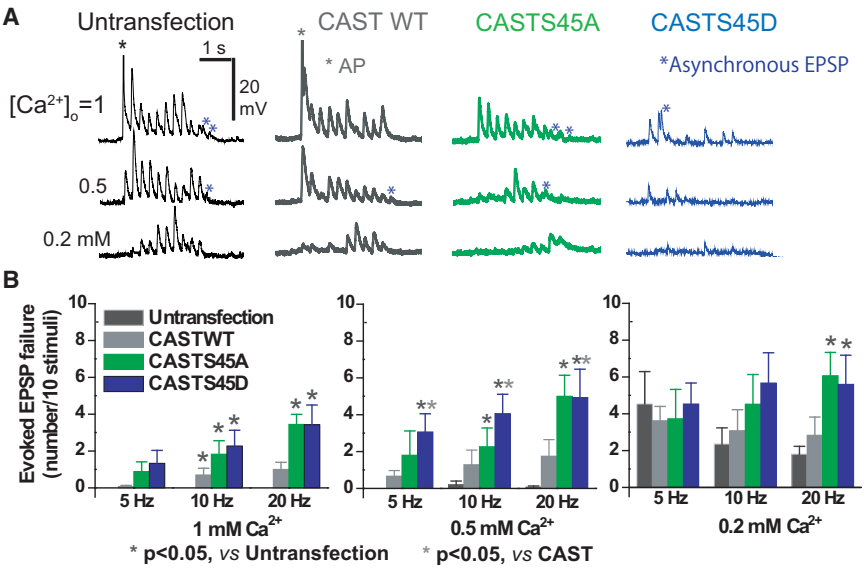

Figure 7. CAST Overexpression Reduced SV Release Efficacy in Low Ca^{2+}

(A) Representative EPSPs were evoked by consecutive ten-AP train at 5 Hz in 1, 0.5, and 0.2 mM Ca^{2+}. Gray*, the EPSP in response to the first presynaptic AP generated an AP (out of scale) in un- and CAST-transfected synapses; blue*, EPSP generated asynchronously.

(B) Ca^{2+} dependence of CAST function. EPSPs in response to ten-APs train at 5, 10, and 20 Hz generated in presynaptic neurons expressing $CAST^{WT}$ or $CAST^{S45}$ mutants were recorded three times every 1 min. The recording was performed continuously by changing external solutions containing 1, 0.5, and 0.2 mM Ca^{2+}. EPSP failures in each Ca^{2+}solution were averaged (n = 5–6; *p < 0.05, unpaired t test; dark gray*, versus untransfection; gray*, versus CAST overexpression). Error bars represent SEM.

2002]), augmentation (Munc-13 [Rhee et al., 2002; Rosenmund et al., 2002]), PTP (RIM1α [Schoch et al., 2002]), and synaptic depression (RIM1α [Calakos et al., 2004]; Bassoon [Hallermann et al., 2010]). CAST upregulates synaptic efficacy in response to repetitive activity at inhibitory synapses (Kaeser et al., 2009). While the absence of AZ proteins can alter synaptic plasticity, AZ proteins that form a complex may functionally regulate synaptic release probability and synaptic efficacy. Our study suggests that CAST controls short-term synaptic depression induced within 200 ms following an AP (Figure 5), but not in slower forms of presynaptic plasticity, such as augmentation or PTP (Figure 6).

Normally, lower basal release probability results in a large augmentation ratio. It is therefore surprising that after a 20-Hz train for 10 s there is no difference in the augmentation ratio between $CAST^{WT}$ (release probability 0.27) and untransfected neurons (release probability 0.61), whereas there is a massive reduction for $CAST^{S45D}$ (release probability 0.75). Interestingly, in lower Ca^{2+}, the second EPSP size of $CAST^{WT}$ is much smaller and the EPSP failure to ten APs is more than that of untransfected synapses (Figure 7A). Presynaptic short-term plasticity is regulated by residual Ca^{2+} after AP firing (Zucker and Regehr, 2002). The function of CAST in controlling RRP reloading shortly after AP firing (Figure 5) and in the maintenance of transmitter release during high-frequency AP firing (Figures 6C and 7) suggest that both are dependent on the Ca^{2+} concentration at the AZ, despite the absence of a canonical Ca^{2+}-binding site. These data suggest that Ca^{2+} sensors may control AZ homeostasis upstream of the SAD kinase, which provides a more selective signal to CAST complexes.

CAST Controls Rapid and Complete Reloading of the RRP

Among AZ proteins, Bassoon controls the speed of rapid reloading of the RRP with SVs during high-frequency transmission, although it is not involved in slow reloading or in basal transmitter release (Hallermann et al., 2010). Neither RIM1α nor CAST controls RRP reloading in cultured hippocampal neurons (Calakos et al., 2004; Kaeser et al., 2009). In both these reports, the RRP reloading was measured by the application of hypertonic sucrose; in a previous study, we showed that the RRP measured by a 2-s puff application of 0.5 M sucrose was 2.7-fold larger than that measured by 2-s AP trains at 50 Hz (Ma et al., 2009). For the measurement of RRP reloading following CAST deletion, hypertonic solution was applied for 60 s (Kaeser et al., 2009); in the present study, we applied sucrose for 10 s and found no difference in RRP reloading between the phosphonegative form and phosphomimetic CAST expression (Figures 3G–3J). Thus, we propose that $CAST^{S45}$ phosphorylation controls physiological RRP reloading. Our work shows that $CAST^{S45}$ phosphorylation controls both rapid and slow reloading of the RRP after depletion (Figure 4), suggesting that phosphorylated $CAST^{S45}$ controls the final step of SV reloading to a common RRP for both rapid and slow SV-recycling pathways.

Conclusions

Collectively, our findings provide a foundation for understanding the molecular mechanisms responsible for AZ regulation of SV reloading into the RRP in response to AP input. We propose that CAST controls the speed of SV reloading to the release sites, within 200 ms following each AP input, to maintain the general capability for stable signal transmission. CAST phosphorylation by SAD kinase during high rates of synaptic activity may allow synapses to respond dynamically to rapid or complex AP patterns, by constraining release from a smaller RRP to induce short-term synaptic depression and support the sustainability of synaptic resources during prolonged or intense neural circuit activity.

EXPERIMENTAL PROCEDURES

Ethical Approval

The Ethics Committee of Tokyo Medical University approved the project. The use of transgenic mice was approved by the Institutional Committee for the

Care and Use of Experimental Animals at the University of Yamanashi and Niigata University.

Constructs and Recombinant Kinase Domains

The constructs of SAD-B were described previously (Inoue et al., 2006). Expression vectors were constructed in pMALc2 vector (New England Biolabs) by standard molecular biological methods. These MBP-fusion proteins were purified from *Escherichia coli* according to the manufacturer's protocol.

shRNAs

Oligonucleotides were annealed and ligated into pSUPER.RFP vector (Ageta-Ishihara et al., 2009), a kind gift from Dr. H. Bito, The University of Tokyo. Sequences of shRNA were as follows: control shRNA, 5′-GAAACG GAAAGCAGGTACG-3′; shRNA 1392, 5′-GCTTGAAACCCTTAGCAAT-3′; and shRNA 1428, 5′-GCAACACATTGAAGTGCTT-3′. The efficiencies of respective shRNAs were determined in HEK293T cells by cotransfection with pCIneo-myc-rCAST (Ohtsuka et al., 2002) using polyethylenimine. Three days after transfection, proteins were extracted and subjected to immunoblot analysis. The intensities of bands for CAST were quantified and normalized with those for red fluorescent protein (RFP).

Antibodies

A polyclonal anti-phosphospecific antibody (anti-p-CAST) was raised against TGKTL (phospho-S)MENI coupled to keyhole limpet hemocyanin via the N-terminal cysteine residues (Operon Biotechnologies). The polyclonal anti-CAST and ELKS antibodies were obtained as described (Takao-Rikitsu et al., 2004). The monoclonal antibodies for Bassoon (Enzo Life Sciences) and PSD-95 (Chemicon) were purchased from commercial sources.

Kinase Assay

The kinase assay was performed as described previously (Inoue et al., 2006). Briefly, various GST-fusion proteins of CAST were incubated with indicated recombinant kinase domains (1–5 μg protein each) in 50 μl kinase buffer containing 50 mM Tris/HCl (pH 7.5), 0.1% Triton X-100, 1 mM DTT, 100 mM NaCl, 10 mM $MgCl_2$, and 1 μCi [γ-^{32}P] ATP. After incubation for 45 min at 30°C, the reaction was stopped with 25 μl 3× SDS-PAGE sample buffer and subjected to SDS-PAGE followed by autoradiography. For western blotting, the kinase assay was performed in a reaction mixture containing 200 μM ATP (GE Healthcare) without [γ-^{32}P] ATP.

Subcellular Fractionation

To obtain the SM3 and PSD fractions, subcellular fractionation of rat brain was performed as described previously (Inoue et al., 2006; Ohtsuka et al., 2002). In brief, the synaptosomal membrane fraction was centrifuged at 48,200 × *g* at 4°C and purified on a set of sucrose density gradients consisting of 0.85, 1.0, and 1.2 M sucrose. The band between 1.0 and 1.2 M sucrose was collected and used as the SM3 fraction. This fraction contains the pre- and postsynaptic membranes plus the PSD and docked vesicles. The SM3 fraction was treated with 1% (w/v) Triton X-100 and further centrifuged at 48,200 × *g* at 4°C. The resultant pellet was used as the PSD fraction.

To obtain the crude membrane fractions, subcellular fractionation of mouse brain (0.3 g) was performed as described previously with modifications (Ohtsuka et al., 2002). In brief, brain homogenates were centrifuged at 800 × *g*. The supernatant (S1) was centrifuged at 9,200 × *g*, and the resultant pellet was washed and homogenized in buffer A (4 mM HEPES [pH 7.3], 0.32 M sucrose, and complete protease inhibitor [Roche]) and then used as the crude membrane fraction (P2).

Immunohistochemistry of the Mouse Hippocampus

Immunohistochemistry of the mouse hippocampus was performed as previously described (Furuse et al., 1993). In brief, frozen brains were sectioned at 20-μm thickness in the sagittal plane using a cryostat, and they were fixed in 95% ethanol at 4°C for 30 min and in acetone at room temperature for 1 min. After blocking with 2% normal goat serum and 0.2% (w/v) Triton X-100 in PBS for 30 min, sections were incubated with anti-p-CAST (1:200) and anti-CAST (1:200) antibodies overnight. Then they were incubated with Alexa Fluor 568- and 488-labeled species-specific secondary antibodies (1:500, Molecular Probes). Images were captured with a confocal laser-scanning microscope (FV1200, Olympus).

Immunofluorescence Staining of SCG Neurons

SCG neurons 5 weeks in culture were prepared as described previously (Ma and Mochida, 2007). Anti-p-CAST and -CAST antibodies and anti-Bassoon antibody (Enzo Life Sciences) were used for the primary antibody. Alexa Fluor 448 goat anti-guinea pig IgG or 546 goat anti-guinea pig IgG, Alexa Fluor 448 goat anti-rabbit IgG or 546 donkey anti-rabbit IgG, and Alexa Fluor 488 goat anti-mouse IgG or 546 rabbit anti-mouse IgG (A11073 or A-11074, A-11008 or A10040, and A-11001 or A11060; Molecular Probes; 1:500) were used for the secondary antibody.

Confocal images were obtained with a Nikon EZ-C1 using water immersion 60× objective. Images were acquired using settings below saturation at a resolution of 1,024 × 1,024 pixels (12 bit), and the density of p-CAST and CAST was quantified by averaging the fluorescence intensity within five circles (1 μm^2 each) around a cell body in images containing two neurons, using MetaMorph Software (Molecular Devices). For Figure 2D, we performed immunostaining using four cultures and measured the fluorescence intensity of phosphorylated CAST or ELKS and then that of Bassoon. Images of four to ten neuron pairs in each performance were quantitatively analyzed. For Figures 2E and 2F, we performed immunostaining using two cultures and measured the fluorescence intensity of CAST and then of phosphorylated CAST. Images of five to 14 neuron pairs were analyzed for the quantitative experiments. The area measurement for the comparison of the Bassoon distribution with or without CAST phosphorylation mutants (Figure 3A) was performed using three cultures each. Five areas of Bassoon alone and areas around CAST fluorescence in images of three to five neuron pairs in each performance were analyzed with a Nikon C2 confocal imaging system.

Electrophysiology

SCG neurons were cultured as described previously (Ma and Mochida, 2007) to allow synapse formation, and cDNAs encoding EGFP-CAST, the pCAEGFP mutants (Inoue et al., 2006), or pSUPER.RFP vectors containing shRNAs for CAST were microinjected into the nuclei of SCG neurons after 5 weeks in cell culture as described (Ma et al., 2009; Ma and Mochida, 2007). Then 2–4 days after the transfection, by generating AP in a transfected presynaptic SCG neuron with a sharp microelectrode filled with 1 M K-acetate (70–90 MΩ), EPSPs were recorded from a neighboring untransfected SCG neuron with another sharp microelectrode (Ma et al., 2009; Ma and Mochida, 2007), using an extracellular solution with different calcium concentrations. Details of these solutions are presented in the figure legends. Data were collected using Clampex 10.2 (Molecular Devices) and analyzed with Origin software (OriginLab).

Analysis of EPSPs with Various AP Firing Patterns

The Rise Time of EPSP

The voltage change from one-third to two-thirds of peak amplitude was divided by the time.

The RRP Size

The RRP size was estimated from back-extrapolation (to time = 0) of average cumulative EPSP integral recorded at 50 Hz (Ma et al., 2009) using Origin 8. The number of SVs in the RRP was estimated by dividing the value at t = 0 by the mean cumulative integral value of the quantal EPSP (0.019 mV; Krapivinsky et al., 2006). Also, 0.5 M sucrose was puff-applied to presynaptic neurons every 4 min (Mochida et al., 1998; Baba et al., 2005; Hayashida et al., 2015). Sucrose responses were recorded five times with Clampex; integral values measured by Clampfit (pClamp 10, Molecular Devices) were averaged. The values from untransfected or transfected synapses were averaged. The integral values were normalized.

RRP Depletion and Recovery

EPSP was recorded at 0.5 Hz. After a 1-min control recording at 0.5 Hz, a 5-min stimulation at 5 Hz was applied to deplete SVs in the RRP. EPSP amplitudes were normalized to the mean EPSP amplitude before the AP trains.

Time Constant for RRP Recovery

Averaged EPSP amplitudes were fitted with single exponential growth curves by 8 s and with linear lines by 9 min after the AP train, using Origin 7.5

exponential growth and linear fits. To show clearly the fast recovery rate, the mean value of noise level of the baseline recording at time = 0 (<1 mV) was subtracted from the mean EPSP amplitudes.

Paired-Pulse Ratio

To examine release-ready SVs following AP generation, two consecutive APs at various ISIs were elicited, every 1 min, in the cDNA- or shRNA-transfected neurons. Recordings for each ISI were performed in triplicate. To calculate the paired-pulse ratio, the second EPSP amplitude measured from the end of the first EPSP was normalized by the amplitude of the first EPSP measured from the baseline before generating the first EPSP. The mean values of the paired-pulse ratio for individual synapses were calculated.

Statistics

Statistical significance was determined using two-tailed Student's t tests or one-way ANOVA. All data are shown as the mean with SEM. Statistical significance was assumed when $p < 0.05$, $p < 0.01$, or $p < 0.001$.

SUPPLEMENTAL INFORMATION

Supplemental Information includes Supplemental Experimental Procedures and three figures and can be found with this article online at http://dx.doi.org/10.1016/j.celrep.2016.08.020.

AUTHOR CONTRIBUTIONS

S.M. designed and performed electrophysiology and immunocytochemistry experiments with SCG neurons, analyzed data, and wrote the paper. S.T. maintained the cultured SCG neurons, performed immunocytochemistry, and analyzed the data. H.M. performed electrophysiology experiments. K.S. and M.A. generated the knockin mice. A.H. and S.H. performed immunohistochemistry and immunocytochemistry experiments and analyzed the data. Y.H., M.Y., H.M., and I.K. performed biochemistry experiments. T.O. designed biochemistry experiments, analyzed data, and wrote the paper.

ACKNOWLEDGMENTS

This work was supported by grants-in-aid for Scientific Research B and for Exploratory Research (S.M. and T.O.) and the Daiichi Sankyo Foundation of Life Science and the Toray Science Foundation (T.O.). We thank S. Higa for his contribution to the early stage of this work. We also thank H. Bito and H. Hioki for the pSUPER.mRFP and palGFP vectors, respectively.

Received: December 14, 2015
Revised: June 28, 2016
Accepted: August 5, 2016
Published: September 13, 2016

REFERENCES

Ageta-Ishihara, N., Takemoto-Kimura, S., Nonaka, M., Adachi-Morishima, A., Suzuki, K., Kamijo, S., Fujii, H., Mano, T., Blaeser, F., Chatila, T.A., et al. (2009). Control of cortical axon elongation by a GABA-driven Ca^{2+}/calmodulin-dependent protein kinase cascade. J. Neurosci. *29*, 13720–13729.

Baba, T., Sakisaka, T., Mochida, S., and Takai, Y. (2005). PKA-catalyzed phosphorylation of tomosyn and its implication in Ca^{2+}-dependent exocytosis of neurotransmitter. J. Cell Biol. *170*, 1113–1125.

Beierlein, M., Fioravante, D., and Regehr, W.G. (2007). Differential expression of posttetanic potentiation and retrograde signaling mediate target-dependent short-term synaptic plasticity. Neuron *54*, 949–959.

Betz, A., Thakur, P., Junge, H.J., Ashery, U., Rhee, J.S., Scheuss, V., Rosenmund, C., Rettig, J., and Brose, N. (2001). Functional interaction of the active zone proteins Munc13-1 and RIM1 in synaptic vesicle priming. Neuron *30*, 183–196.

Brager, D.H., Cai, X., and Thompson, S.M. (2003). Activity-dependent activation of presynaptic protein kinase C mediates post-tetanic potentiation. Nat. Neurosci. *6*, 551–552.

Branco, T., Marra, V., and Staras, K. (2010). Examining size-strength relationships at hippocampal synapses using an ultrastructural measurement of synaptic release probability. J. Struct. Biol. *172*, 203–210.

Brose, N., Hofmann, K., Hata, Y., and Südhof, T.C. (1995). Mammalian homologues of Caenorhabditis elegans unc-13 gene define novel family of C2-domain proteins. J. Biol. Chem. *270*, 25273–25280.

Browning, M.D., Huganir, R., and Greengard, P. (1985). Protein phosphorylation and neuronal function. J. Neurochem. *45*, 11–23.

Calakos, N., Schoch, S., Südhof, T.C., and Malenka, R.C. (2004). Multiple roles for the active zone protein RIM1alpha in late stages of neurotransmitter release. Neuron *42*, 889–896.

Del Castillo, J., and Katz, B. (1954). Quantal components of the end-plate potential. J. Physiol. *124*, 560–573.

Deng, L., Kaeser, P.S., Xu, W., and Südhof, T.C. (2011). RIM proteins activate vesicle priming by reversing autoinhibitory homodimerization of Munc13. Neuron *69*, 317–331.

Fenster, S.D., Chung, W.J., Zhai, R., Cases-Langhoff, C., Voss, B., Garner, A.M., Kaempf, U., Kindler, S., Gundelfinger, E.D., and Garner, C.C. (2000). Piccolo, a presynaptic zinc finger protein structurally related to bassoon. Neuron *25*, 203–214.

Furuse, M., Hirase, T., Itoh, M., Nagafuchi, A., Yonemura, S., Tsukita, S., and Tsukita, S. (1993). Occludin: a novel integral membrane protein localizing at tight junctions. J. Cell Biol. *123*, 1777–1788.

Gillis, K.D., Mossner, R., and Neher, E. (1996). Protein kinase C enhances exocytosis from chromaffin cells by increasing the size of the readily releasable pool of secretory granules. Neuron *16*, 1209–1220.

Hallermann, S., Fejtova, A., Schmidt, H., Weyhersmüller, A., Silver, R.A., Gundelfinger, E.D., and Eilers, J. (2010). Bassoon speeds vesicle reloading at a central excitatory synapse. Neuron *68*, 710–723.

Han, Y., Kaeser, P.S., Südhof, T.C., and Schneggenburger, R. (2011). RIM determines Ca^{2+} channel density and vesicle docking at the presynaptic active zone. Neuron *69*, 304–316.

Hanse, E., and Gustafsson, B. (2001). Vesicle release probability and pre-primed pool at glutamatergic synapses in area CA1 of the rat neonatal hippocampus. J. Physiol. *531*, 481–493.

Hardie, D.G. (2007). AMP-activated/SNF1 protein kinases: conserved guardians of cellular energy. Nat. Rev. Mol. Cell Biol. *8*, 774–785.

Hayashida, M., Tanifuji, S., Ma, H., Murakami, N., and Mochida, S. (2015). Neural activity selects myosin IIB and VI with a specific time window in distinct dynamin isoform-mediated synaptic vesicle reuse pathways. J. Neurosci. *35*, 8901–8913.

Inoue, E., Mochida, S., Takagi, H., Higa, S., Deguchi-Tawarada, M., Takao-Rikitsu, E., Inoue, M., Yao, I., Takeuchi, K., Kitajima, I., et al. (2006). SAD: a presynaptic kinase associated with synaptic vesicles and the active zone cytomatrix that regulates neurotransmitter release. Neuron *50*, 261–275.

Kaeser, P.S., Deng, L., Chávez, A.E., Liu, X., Castillo, P.E., and Südhof, T.C. (2009). ELKS2alpha/CAST deletion selectively increases neurotransmitter release at inhibitory synapses. Neuron *64*, 227–239.

Kittel, R.J., Wichmann, C., Rasse, T.M., Fouquet, W., Schmidt, M., Schmid, A., Wagh, D.A., Pawlu, C., Kellner, R.R., Willig, K.I., et al. (2006). Bruchpilot promotes active zone assembly, Ca^{2+} channel clustering, and vesicle release. Science *312*, 1051–1054.

Krapivinsky, G., Mochida, S., Krapivinsky, L., Cibulsky, S.M., and Clapham, D.E. (2006). The TRPM7 ion channel functions in cholinergic synaptic vesicles and affects transmitter release. Neuron *52*, 485–496.

Landis, D.M., Hall, A.K., Weinstein, L.A., and Reese, T.S. (1988). The organization of cytoplasm at the presynaptic active zone of a central nervous system synapse. Neuron *1*, 201–209.

Leal, K., Mochida, S., Scheuer, T., and Catterall, W.A. (2012). Fine-tuning synaptic plasticity by modulation of Ca(V)2.1 channels with Ca^{2+} sensor proteins. Proc. Natl. Acad. Sci. USA *109*, 17069–17074.

Lonart, G., Schoch, S., Kaeser, P.S., Larkin, C.J., Südhof, T.C., and Linden, D.J. (2003). Phosphorylation of RIM1alpha by PKA triggers presynaptic long-term potentiation at cerebellar parallel fiber synapses. Cell *115*, 49–60.

Lu, W., Ma, H., Sheng, Z.H., and Mochida, S. (2009). Dynamin and activity regulate synaptic vesicle recycling in sympathetic neurons. J. Biol. Chem. *284*, 1930–1937.

Ma, H., and Mochida, S. (2007). A cholinergic model synapse to elucidate protein function at presynaptic terminals. Neurosci. Res. *57*, 491–498.

Ma, H., Cai, Q., Lu, W., Sheng, Z.H., and Mochida, S. (2009). KIF5B motor adaptor syntabulin maintains synaptic transmission in sympathetic neurons. J. Neurosci. *29*, 13019–13029.

Manning, G., Whyte, D.B., Martinez, R., Hunter, T., and Sudarsanam, S. (2002). The protein kinase complement of the human genome. Science *298*, 1912–1934.

Mochida, S. (2011). Activity-dependent regulation of synaptic vesicle exocytosis and presynaptic short-term plasticity. Neurosci. Res. *70*, 16–23.

Mochida, S., Kobayashi, H., Matsuda, Y., Yuda, Y., Muramoto, K., and Nonomura, Y. (1994). Myosin II is involved in transmitter release at synapses formed between rat sympathetic neurons in culture. Neuron *13*, 1131–1142.

Mochida, S., Yokoyama, C.T., Kim, D.K., Itoh, K., and Catterall, W.A. (1998). Evidence for a voltage-dependent enhancement of neurotransmitter release mediated via the synaptic protein interaction site of N-type Ca2+ channels. Proc. Natl. Acad. Sci. USA *95*, 14523–14528.

Mochida, S., Few, A.P., Scheuer, T., and Catterall, W.A. (2008). Regulation of presynaptic Ca(V)2.1 channels by Ca^{2+} sensor proteins mediates short-term synaptic plasticity. Neuron *57*, 210–216.

Mori, M., Tanifuji, S., and Mochida, S. (2014). Kinetic organization of Ca^{2+} signals that regulate synaptic release efficacy in sympathetic neurons. Mol. Pharmacol. *86*, 297–305.

Nestler, E.J., and Greengard, P. (1982). Nerve impulses increase the phosphorylation state of protein I in rabbit superior cervical ganglion. Nature *296*, 452–454.

Ohtsuka, T., Takao-Rikitsu, E., Inoue, E., Inoue, M., Takeuchi, M., Matsubara, K., Deguchi-Tawarada, M., Satoh, K., Morimoto, K., Nakanishi, H., and Takai, Y. (2002). Cast: a novel protein of the cytomatrix at the active zone of synapses that forms a ternary complex with RIM1 and munc13-1. J. Cell Biol. *158*, 577–590.

Peters, M., Mizuno, K., Ris, L., Angelo, M., Godaux, E., and Giese, K.P. (2003). Loss of Ca^{2+}/calmodulin kinase kinase beta affects the formation of some, but not all, types of hippocampus-dependent long-term memory. J. Neurosci. *23*, 9752–9760.

Rhee, J.S., Betz, A., Pyott, S., Reim, K., Varoqueaux, F., Augustin, I., Hesse, D., Südhof, T.C., Takahashi, M., Rosenmund, C., and Brose, N. (2002). Beta phorbol ester- and diacylglycerol-induced augmentation of transmitter release is mediated by Munc13s and not by PKCs. Cell *108*, 121–133.

Rizzoli, S.O., and Betz, W.J. (2005). Synaptic vesicle pools. Nat. Rev. Neurosci. *6*, 57–69.

Rosenmund, C., Sigler, A., Augustin, I., Reim, K., Brose, N., and Rhee, J.S. (2002). Differential control of vesicle priming and short-term plasticity by Munc13 isoforms. Neuron *33*, 411–424.

Schikorski, T., and Stevens, C.F. (2001). Morphological correlates of functionally defined synaptic vesicle populations. Nat. Neurosci. *4*, 391–395.

Schoch, S., Castillo, P.E., Jo, T., Mukherjee, K., Geppert, M., Wang, Y., Schmitz, F., Malenka, R.C., and Südhof, T.C. (2002). RIM1alpha forms a protein scaffold for regulating neurotransmitter release at the active zone. Nature *415*, 321–326.

Takao-Rikitsu, E., Mochida, S., Inoue, E., Deguchi-Tawarada, M., Inoue, M., Ohtsuka, T., and Takai, Y. (2004). Physical and functional interaction of the active zone proteins, CAST, RIM1, and Bassoon, in neurotransmitter release. J. Cell Biol. *164*, 301–311.

Tanifuji, S., Funakoshi-Tago, M., Ueda, F., Kasahara, T., and Mochida, S. (2013). Dynamin isoforms decode action potential firing for synaptic vesicle recycling. J. Biol. Chem. *288*, 19050–19059.

tom Dieck, S., Sanmartí-Vila, L., Langnaese, K., Richter, K., Kindler, S., Soyke, A., Wex, H., Smalla, K.H., Kämpf, U., Fränzer, J.T., et al. (1998). Bassoon, a novel zinc-finger CAG/glutamine-repeat protein selectively localized at the active zone of presynaptic nerve terminals. J. Cell Biol. *142*, 499–509.

tom Dieck, S., Specht, D., Strenzke, N., Hida, Y., Krishnamoorthy, V., Schmidt, K.-F., Inoue, E., Ishizaki, H., Tanaka-Okamoto, M., Miyoshi, J., et al. (2012). Deletion of the presynaptic scaffold CAST reduces active zone size in rod photoreceptors and impairs visual processing. J. Neurosci. *32*, 12192–12203.

Wagh, D.A., Rasse, T.M., Asan, E., Hofbauer, A., Schwenkert, I., Dürrbeck, H., Buchner, S., Dabauvalle, M.C., Schmidt, M., Qin, G., et al. (2006). Bruchpilot, a protein with homology to ELKS/CAST, is required for structural integrity and function of synaptic active zones in Drosophila. Neuron *49*, 833–844.

Wang, Y., Okamoto, M., Schmitz, F., Hofmann, K., and Südhof, T.C. (1997). Rim is a putative Rab3 effector in regulating synaptic-vesicle fusion. Nature *388*, 593–598.

Wang, X., Kibschull, M., Laue, M.M., Lichte, B., Petrasch-Parwez, E., and Kilimann, M.W. (1999). Aczonin, a 550-kD putative scaffolding protein of presynaptic active zones, shares homology regions with Rim and Bassoon and binds profilin. J. Cell Biol. *147*, 151–162.

Wang, Y., Liu, X., Biederer, T., and Südhof, T.C. (2002). A family of RIM-binding proteins regulated by alternative splicing: Implications for the genesis of synaptic active zones. Proc. Natl. Acad. Sci. USA *99*, 14464–14469.

Weyhersmüller, A., Hallermann, S., Wagner, N., and Eilers, J. (2011). Rapid active zone remodeling during synaptic plasticity. J. Neurosci. *31*, 6041–6052.

Wojcik, S.M., and Brose, N. (2007). Regulation of membrane fusion in synaptic excitation-secretion coupling: speed and accuracy matter. Neuron *55*, 11–24.

Zucker, R.S., and Regehr, W.G. (2002). Short-term synaptic plasticity. Annu. Rev. Physiol. *64*, 355–405.